SCIENTIFIC REPORTS

OPEN

SUBJECT AREAS:
PEPTIDES
DRUG DEVELOPMENT

Received
24 December 2013

Accepted
12 March 2014

Published
28 March 2014

Correspondence and requests for materials should be addressed to S.K. (serdar@physics.usyd.edu.au) or R.S.N. (ray.norton@monash.edu)

A potent and Kv1.3-selective analogue of the scorpion toxin HsTX1 as a potential therapeutic for autoimmune diseases

M. Harunur Rashid[1,2], Redwan Huq[3,4], Mark R. Tanner[3,5], Sandeep Chhabra[1], Keith K. Khoo[1], Rosendo Estrada[6], Vikas Dhawan[6], Satendra Chauhan[6], Michael W. Pennington[6], Christine Beeton[3], Serdar Kuyucak[2] & Raymond S. Norton[1]

[1]Medicinal Chemistry, Monash Institute of Pharmaceutical Sciences, Monash University, Parkville, Victoria 3052Australia, [2]School of Physics, University of Sydney, New South Wales 2006, Australia, [3]Department of Molecular Physiology and Biophysics, Baylor College of Medicine, Houston, TX 77030, USA, [4]Graduate Program in Molecular Physiology and Biophysics, Baylor College of Medicine, Houston, TX 77030, USA, [5]Interdepartmental Graduate Program in Translational Biology and Molecular Medicine, Baylor College of Medicine, Houston, TX 77030, USA, [6]Peptides International, 11621 Electron Drive, Louisville, KY 40299, USA.

HsTX1 toxin, from the scorpion *Heterometrus spinnifer*, is a 34-residue, C-terminally amidated peptide cross-linked by four disulfide bridges. Here we describe new HsTX1 analogues with an Ala, Phe, Val or Abu substitution at position 14. Complexes of HsTX1 with the voltage-gated potassium channels Kv1.3 and Kv1.1 were created using docking and molecular dynamics simulations, then umbrella sampling simulations were performed to construct the potential of mean force (PMF) of the ligand and calculate the corresponding binding free energy for the most stable configuration. The PMF method predicted that the R14A mutation in HsTX1 would yield a $>$ 2 kcal/mol gain for the Kv1.3/Kv1.1 selectivity free energy relative to the wild-type peptide. Functional assays confirmed the predicted selectivity gain for HsTX1[R14A] and HsTX1[R14Abu], with an affinity for Kv1.3 in the low picomolar range and a selectivity of more than 2,000-fold for Kv1.3 over Kv1.1. This remarkable potency and selectivity for Kv1.3, which is significantly up-regulated in activated effector memory cells in humans, suggest that these analogues represent valuable leads in the development of therapeutics for autoimmune diseases.

The voltage-gated potassium channel Kv1.3 is significantly up-regulated in activated effector memory (T_{EM}) cells in humans[1,2]. As a consequence, Kv1.3 blockers constitute valuable new therapeutic leads for the treatment of autoimmune diseases mediated by T_{EM} cells, such as multiple sclerosis and rheumatoid arthritis[1–4].

HsTX1 toxin is a 34-residue, C-terminally amidated peptide from the scorpion *Heterometrus spinnifer*, which is cross-linked by four disulfide bridges[5]. Its amino acid sequence and the locations of the four disulfide bridges are shown in Fig. 1. The solution structures of the synthetic toxin[6] and a chimera consisting of the N-terminal half of the closely-related scorpion toxin maurotoxin and the C-terminal half of HsTX1[7] were found to be very similar to the canonical fold adopted by related scorpion toxins that contain only three disulfides, which consists of an N-terminal helix structure connected to a C-terminal two-stranded antiparallel β-sheet.

HsTX1 is a potent blocker of potassium channels. Lebrun et al.[5] found that the peptide inhibited rat Kv1.3 channels with an IC_{50} of *ca* 12 pM and that it did not compete with ^{125}I-apamin for binding to rat brain synaptosomal membranes, although it did compete efficiently with ^{125}I-kaliotoxin for binding to voltage-gated K^+ channels on the same preparation (IC_{50} *ca* 1 pM). It is thus a more potent Kv1.3 channel blocker than maurotoxin and far more specific[5]. Subsequent studies confirmed its marked preference for Kv1.3 over Kv1.1, Kv1.2 and K_{Ca}3.1 channels[7]. This selectivity for Kv1.3 makes HsTX1 a potentially attractive candidate for the treatment of autoimmune diseases such as multiple sclerosis and rheumatoid arthritis, as it has been shown that blockade of this channel in self-reactive T_{EM} cells is effective in preventing the tissue damage associated with these conditions[1–3]. Indeed, a considerable effort has been devoted to developing Kv1.3-selective analogues of the sea anemone peptide ShK as therapeutics for multiple sclerosis[4,8–10] and one of these analogues has recently entered phase 1 clinical trials[11].

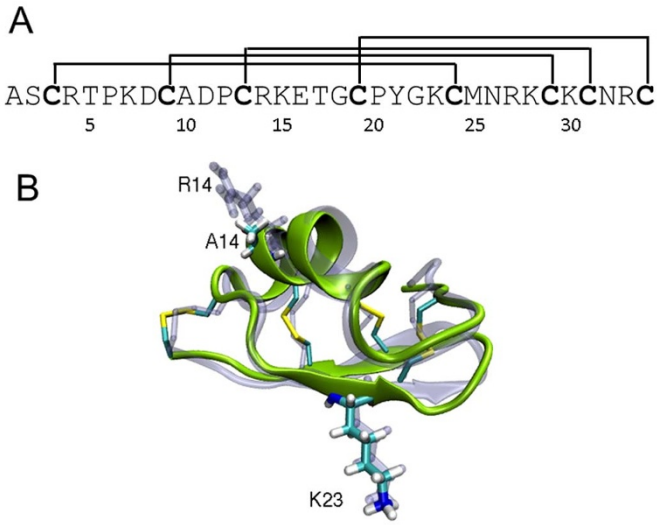

Figure 1 | Structure of HsTX1. (A) Amino acid sequence of HsTX1 (UniProtKB/Swiss-Prot P59867; KAX63_HETSP) showing the positions of the four disulfide bridges[5]. (B) Simulated structure of HsTX1[R14A] (green) superposed on the solution structure of HsTX1[6] (transparent grey) to show that the R14A mutation does not cause any structural changes. Both structures are obtained from equilibrated MD simulations. The side chains of residue 14 and Lys23 in both structures are shown (HsTX1 in grey, HsTX1[R14A] in colour).

In an effort to understand the molecular basis for the potency and selectivity of HsTX1 for Kv1.3, we recently undertook a computational study of its interaction with Kv1.1, 1.2 and 1.3[12]. Accurate models of Kv1.x–HsTX1 complexes were created using docking and molecular dynamics simulations. For each complex, the binding free energy of HsTX1 was determined from the potential of mean force calculations, with good agreement being obtained between the computed and experimental binding free energies. Comparison of the binding modes of HsTX1 with Kv1.1 and Kv1.3 revealed that the lower affinity of HsTX1 for Kv1.1 is due to its inability to come close to the pore domain, which prevents the pore-inserting lysine from making proper contacts with the tyrosine carbonyls in the selectivity filter of the channel.

In this study we have utilized these models to design analogues of HsTX1 with mutations at position 14, which resulted in even greater selectivity for Kv1.3 over Kv1.1 and other channels. Because the R14 mutations perturb the binding mode of HsTX1, the change in binding free energy associated with these mutations may not be reliably calculated using path-independent methods such as free energy perturbation. We therefore performed umbrella sampling molecular dynamics (MD) simulations and determined the binding free energies of the peptide and HsTX1[R14A] from potential of mean force (PMF) calculations. The PMF method predicts that the R14A mutation in HsTX1 will yield a $>$ 2 kcal/mol gain in the Kv1.3/Kv1.1 selectivity free energy relative to the wild-type peptide. Functional assays confirm the predicted selectivity gain for HsTX1[R14A] and other R14 analogues, and suggest that they will be valuable leads in the development of therapeutics for autoimmune diseases.

Results

Interactions of HsTX1[R14A] with Kv1.3 and Kv1.1. The desire to modify HsTX1 at a site distant from its key pharmacophore led us to utilize docking simulations with both Kv1.1 and Kv1.3 to predict residues that would improve selectivity for Kv1.3 over Kv1.1. Comparing the binding modes of HsTX1 with Kv1.1 and Kv1.3[12], we observed that the R14 side chain made an ionic interaction with the E353 side chain in the turret region of Kv1.1 but had no contacts with Kv1.3 residues. This suggested that replacing R14 with a neutral residue could reduce the toxin's affinity for Kv1.1 without affecting its potency for Kv1.3. We therefore explored in this study the effect of replacing R14 in HsTX1 with alternative side chains. Snapshots of the Kv1.x–HsTX1[R14A] complexes are shown in Fig. 2. To facilitate comparison of the binding mode of this analogue with that of the wild-type toxin[12], we have superimposed the Kv1.x–HsTX1 structure on that of HsTX1[R14A] after aligning the two structures. It is evident that, although there are no large rotations, the structure of HsTX1[R14A] is slightly shifted relative to HsTX1. The effects of these changes on the binding modes are quantified in Table 1, which lists the average pair distances for the strongly interacting residues. In Kv1.1, the lost R14 contact is replaced by the N26–Y379 H-bond. In addition, R33 switches from E353 to E351, making a weaker contact. In Kv1.3, there are still five contacts but two of them (Y21 and N26) are replaced by R27 and K30. From the comparison of the binding modes, we expect the R14A mutation to reduce the affinity of the toxin to Kv1.1 but not to Kv1.3, thus improving the Kv1.3/Kv1.1 selectivity margin. To calculate by how much, we constructed the PMFs for the Kv1.x–HsTX1[R14A] complexes.

Umbrella sampling MD simulations were performed as described in our earlier work on binding of toxin peptides to potassium channels[8,9,13,14]. Inspection of the backbone RMSD values of HsTX1[R14A] in each umbrella window showed that they exhibit a similar behaviour to those of HsTX1[12]. Namely, binding suppresses the RMSD values relative to the bulk, but they return to the bulk values after the toxin unbinds (data not shown). Thus, no artificial deformation of the peptide occurs during the PMF calculations. Convergence of the PMFs is demonstrated in supplementary Fig. S1. For Kv1.3, the PMF profile of HsTX1[R14A] and its convergence characteristics are very similar to those of HsTX1 (Figure 5 in Rashid & Kuyucak[12]). Despite weaker binding of HsTX1[R14A] to Kv1.1 relative to HsTX1, its PMF converges much faster. To understand this feature, it is necessary to examine how the pair distances change as the toxin is pulled out. These are shown in supplementary Fig. S2 for both complexes. Comparison of the pair distances for Kv1.3–HsTX1[R14A] with those of Kv1.3–HsTX1 (supplementary Fig. S2) shows that the pair distances exhibit a very similar behaviour in both complexes. In contrast, there is a notable difference between the pair distances in the Kv1.1 complexes. The large fluctuations in the R4 and R33 pair distances seen in the unbinding of HsTX1 occur only for the R4 pair distance in HsTX1[R14A], while R33 dissociates in the first step of pulling and never makes a contact again. The reduction in the side chain fluctuations is presumably responsible for the faster convergence of the Kv1.1–HsTX1[R14A]. More importantly, the R14A mutation caused further destabilization of the binding mode, leading to a rapid detachment of the R33 contact. While this is compensated to a degree by the formation of the N26–Y379 H-bond, we expect the overall effect of the R14A mutation on the binding free energy of the toxin on Kv1.1 to be more than the 2 kcal/mol value associated with the typical loss of a charge contact.

The PMFs for HsTX1[R14A] are compared to those of HsTX1 in Fig. 3, and the absolute binding free energies obtained from the integration of the PMFs are listed in Table 2. The values of R used in the calculation of the binding constants from eq. 1 are 0.72 and 0.70 Å, respectively, for Kv1.1 and Kv1.3. The PMFs for Kv1.3 have almost the same well depth (Fig. 3) and the corresponding binding free energies are also very similar (Table 2). In contrast, the R14A mutation reduced the well depth in Kv1.1 by 3 kcal/mol and increased the binding free energy of the toxin by 2.7 kcal/mol. Both of these results are in line with the qualitative expectations gathered from comparison of the binding modes, namely, that the R14A mutation should not affect the toxin's affinity to Kv1.3 much but should reduce its affinity for Kv1.1. In summary, the R14A mutation has increased the Kv1.3/Kv1.1 selectivity free energy from

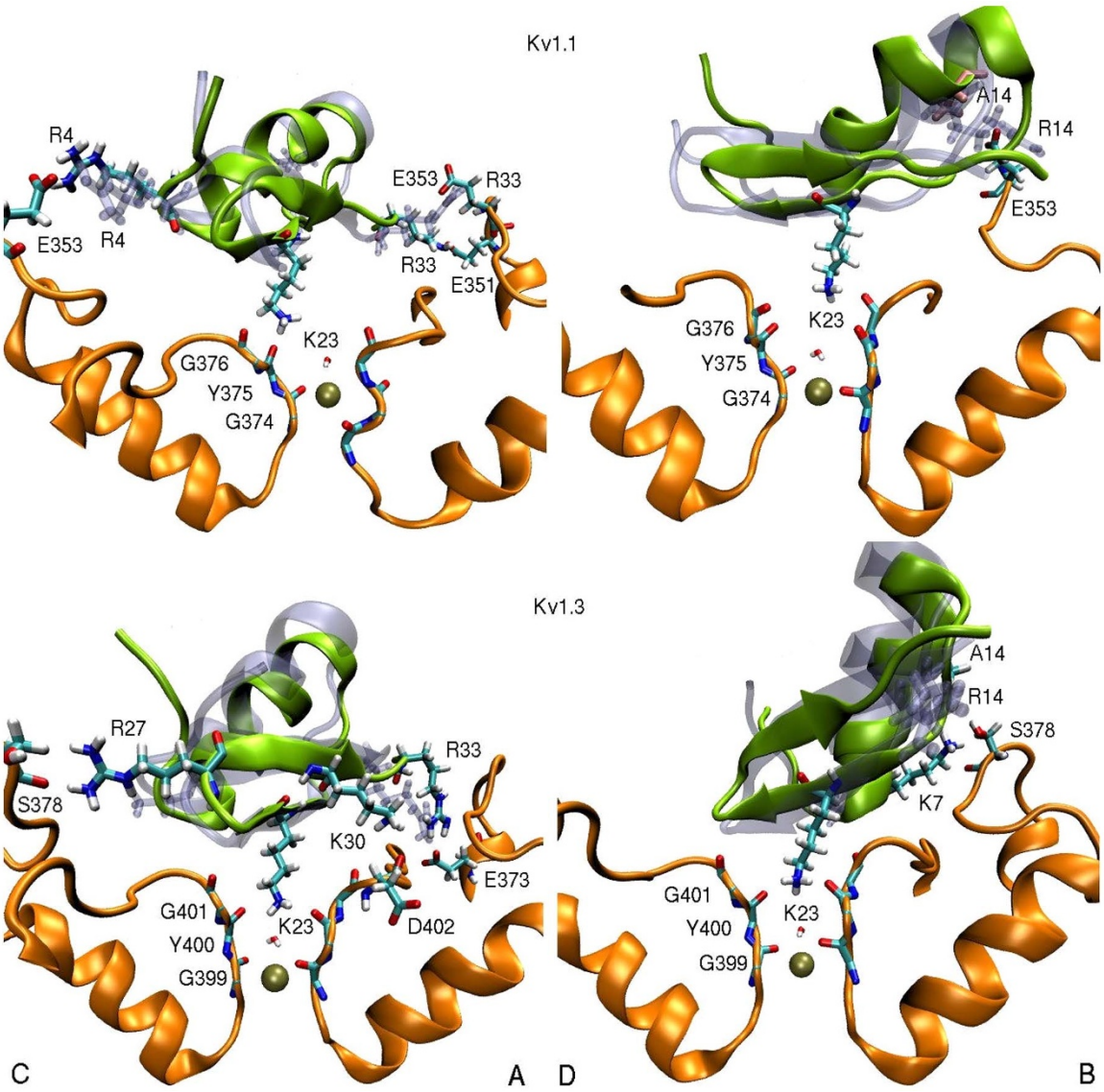

Figure 2 | Interaction of HsTX1[R14A] with potassium channels. Comparison of the binding modes of HsTX1[R14A] (green with coloured side chains) and HsTX1 (transparent grey) in complex with the Kv1.1 and Kv1.3 channels. The R14A mutation causes a small shift in the binding modes of the toxin in both complexes, resulting in some rearrangement of the contact pairs, as documented in the text and Table 1.

3.9 kcal/mol in HsTX1 to 6.2 kcal/mol in HsTX1[R14A]. This is sufficient to render HsTX1[R14A] effectively inactive on Kv1.1.

Peptide synthesis and conformation. In order to confirm the prediction of enhanced selectivity for Kv1.3 over Kv1.1 associated with substitution at Arg14, we replaced this residue in the native sequence with Ala, Abu, Phe or Val. The peptides were assembled using standard Fmoc-tBu solid-phase peptide synthesis. The crude products were oxidized using the glutathione-mediated oxidative folding conditions that have been used successfully for many other ShK analogues[8,10,15]. As shown in Fig. 4, HsTX1[R14A] folded rapidly to a single major product, resulting in the typical pattern of a major earlier-eluting peak by RP-HPLC followed by later-eluting misfolded species and side-products. Each HsTX1 analogue was purified to homogeneity by preparative RP-HPLC, as illustrated in Fig. 4 for HsTX1[R14A]. Each peptide had the correct mass by ESI-MS (data not shown), demonstrating that the four disulfide bonds had been formed. The yield was ~40% of theory based upon the starting resin.

CD spectra were acquired on both HsTX1 and HsTX1[R14A] in dilute acetate buffer. Both peptides exhibited minima at around 221 nm and maxima at around 195 nm (data not shown), very similar to those reported by Lebrun et al.[5] and indicative of a folded peptide containing both α-helical and β-sheet secondary structure.

One-dimensional ^{1}H NMR spectra of HsTX1[R14A] showed sharp and well-dispersed resonances similar to those of wild-type HsTX1 (Fig. 5), indicating that the R14A mutation did not cause any significant perturbation of the native structure. To further verify the structural similarity of wild-type HsTX1 and HsTX1[R14A], chemical shift differences from random coil values for backbone amide and H^{α} resonances were plotted (supplementary Table S1 and Fig. S3). This shows that the pattern of chemical shift deviations from random coil for HsTX1[R14A] closely resembles that of wild-type HsTX1, and confirms that the three-dimensional structures are basically the same. A comparison of the wild-type structure[6] with the simulated structure of HsTX1[R14A] is shown in Fig. 1B.

Potency and selectivity of potassium channel blockade. We used whole-cell patch-clamp to experimentally validate the modelling results. We patch-clamped mouse fibroblasts stably expressing either Kv1.3 or Kv1.1 channels. Perfusion of HsTX1 induced a block of both Kv1.3 and Kv1.1 currents with IC_{50}s of 29 ± 3 pM and 11,330 ± 1,329 pM, respectively (Fig. 6A, B). As predicted by the

Table 1 | Comparison of the strongly interacting pair distances in the HsTX1–Kv1.x complexes with those in the HsTX1[R14A] –Kv1.x complexes

HsTX1	Kv1.1	MD average	HsTX1[R14A]	Kv1.1	MD average
R4-N_2	E353-O_2(C)	3.0 ± 0.5	R4-N_2	E353-O_2(C)	2.7 ± 0.3
R14-N_2	E353-O_1(B)	2.9 ± 0.3			
K23-N_1	Y375-O(C)	2.7 ± 0.3	K23-N_1	Y375-O(C)	2.7 ± 0.5
K23-N_1	G376-O(BC)	3.0 ± 0.2	K23-N_1	G376-O(BC)	4.0 ± 0.4
			N26-O_1	Y379-O_H(C)	2.8 ± 0.3
R33-N_2	E353-O_2(A)	2.7 ± 0.4	R33-N_1	E351-O_2(A)	3.0 ± 0.3
HsTX1	Kv1.3	MD average	HsTX1[R14A]	Kv1.3	MD average
T5-$C_{\gamma 2}$	M403-Cε(C)	3.7 ± 0.3			
K7-N_1	S378-O(B)	2.7 ± 0.5	K7-N_1	S378-O(B)	2.8 ± 0.5
Y21-O_H	D402-O_2(B)	2.7 ± 0.2			
K23-N_1	Y400-O(ABC)	2.7 ± 0.3	K23-N_1	Y400-O(BCD)	2.7 ± 0.3
N26-$N_{\delta 2}$	D402-O(D)	2.8 ± 0.4			
			R27-N_2	S378-O(C)	2.7 ± 0.4
			K30-N_1	D402-O(A)	3.0 ± 0.4
R33-N_2	E373-O_2(A)	2.7 ± 0.3	R33-N_2	E373-O_2(A)	2.8 ± 0.3

The average atom-atom distances obtained from the MD simulations are listed in columns 3 and 6 (in units of Å). Subscripts refer to the side chain atoms and the monomer identity is indicated in parentheses.

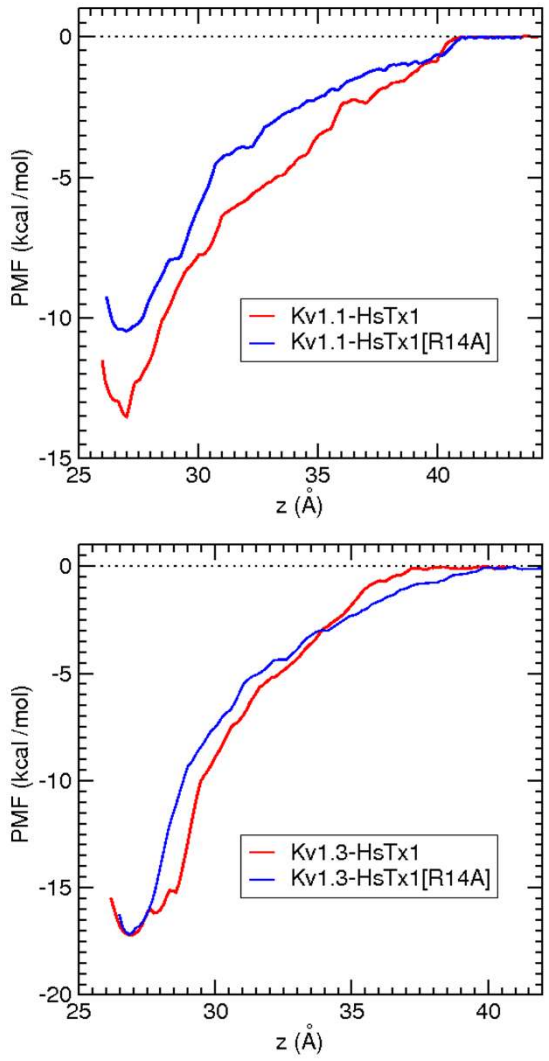

Figure 3 | PMFs for the unbinding of HsTX1[R14A] and HsTX1 from Kv1.1 and Kv1.3. The R14A mutation has little effect on the binding of HsTX1 to Kv1.3 but reduces its affinity for Kv1.1 substantially.

modelling data, HsTX1[R14A] retained its high affinity for Kv1.3 (IC_{50} = 45 ± 3 pM) and exhibited more than 2,000-fold selectivity for Kv1.3 over Kv1.1 with less than 20% Kv1.1 current blocked at a dose of 100 nM (Fig. 6A, B). Substitution of R14 with Abu generated the peptide HsTX1[R14Abu], which displayed a similar affinity and selectivity for Kv1.3 over Kv1.1 with $IC_{50} \approx$ 50 pM on Kv1.3 and > 100 nM on Kv1.1 (data not shown).

Inhibitory effects on lymphocyte proliferation. Since CCR7$^-$ T_{EM} and NA-NK lymphocytes are exquisitely sensitive to Kv1.3 channel block[3,4,16], we tested the effects of HsTX1 and the analogues HsTX1[R14A], HsTX1[R14Abu], HsTX1[R14F] and HsTX1[R14V] on the proliferation of rat CCR7$^-$ T_{EM} cells, rat CCR7$^+$ naïve/T_{CM} cells, and human A-NK and NA-NK cells. As a positive control, we used the well-characterized Kv1.3 channel blocker ShK-186[3,4]. All peptides inhibited the proliferation of Ova-GFP T_{EM} lymphocytes with IC_{50}s ≈ 1 nM (Fig. 6C). In contrast, a concentration of 100 nM of these peptides was necessary to induce a ≈50% block in proliferation of splenic naïve/T_{CM} lymphocytes (Fig. 6C). ShK-186, HsTX1, and its analogues inhibited the mitogen-induced proliferation of NA-NK lymphocytes with IC_{50}s of 5–15 nM but had no significant effect on the proliferation of A-NK cells (Fig. 6D).

Peptide stability. Since HsTX1[R14A] and other R14 analogues displayed high potency and selectivity for Kv1.3 and a corresponding ability to suppress lymphocyte proliferation, we also assessed their resistance to proteolysis *in vitro*. HsTX1[R14A] displayed no sign of degradation in presence of pepsin (Fig. 7A), presumably because of the lack of sequence-specific cleavage sites for this enzyme. In contrast limited digestion (~20%) was observed

Table 2 | Comparison of binding free energies for the HsTX1–Kv1.x and HsTX1[R14A] –Kv1.x complexes

Complex	ΔG_{well}	G_b (PMF)	G_b (exp)[7]
Kv1.1-HsTX1	−13.5 ± 0.3	−10.1 ± 0.3	−11.1 ± 0.1
Kv1.1-HsTX1[R14A]	−10.5 ± 0.3	−7.4 ± 0.3	
Kv1.3-HsTX1	−17.2 ± 0.3	−14.0 ± 0.3	−14.9 ± 0.2
Kv1.3-HsTX1[R14A]	−17.1 ± 0.4	−13.6 ± 0.4	

The relative binding free energies obtained from the well depth in the PMFs are shown in the second column. The standard binding free energies determined from the PMFs using eq 2 (third column) are compared to the experimental values in the last column. Errors in the binding free energies are estimated from the block data analysis of the PMF data. All energies are in kcal/mol.

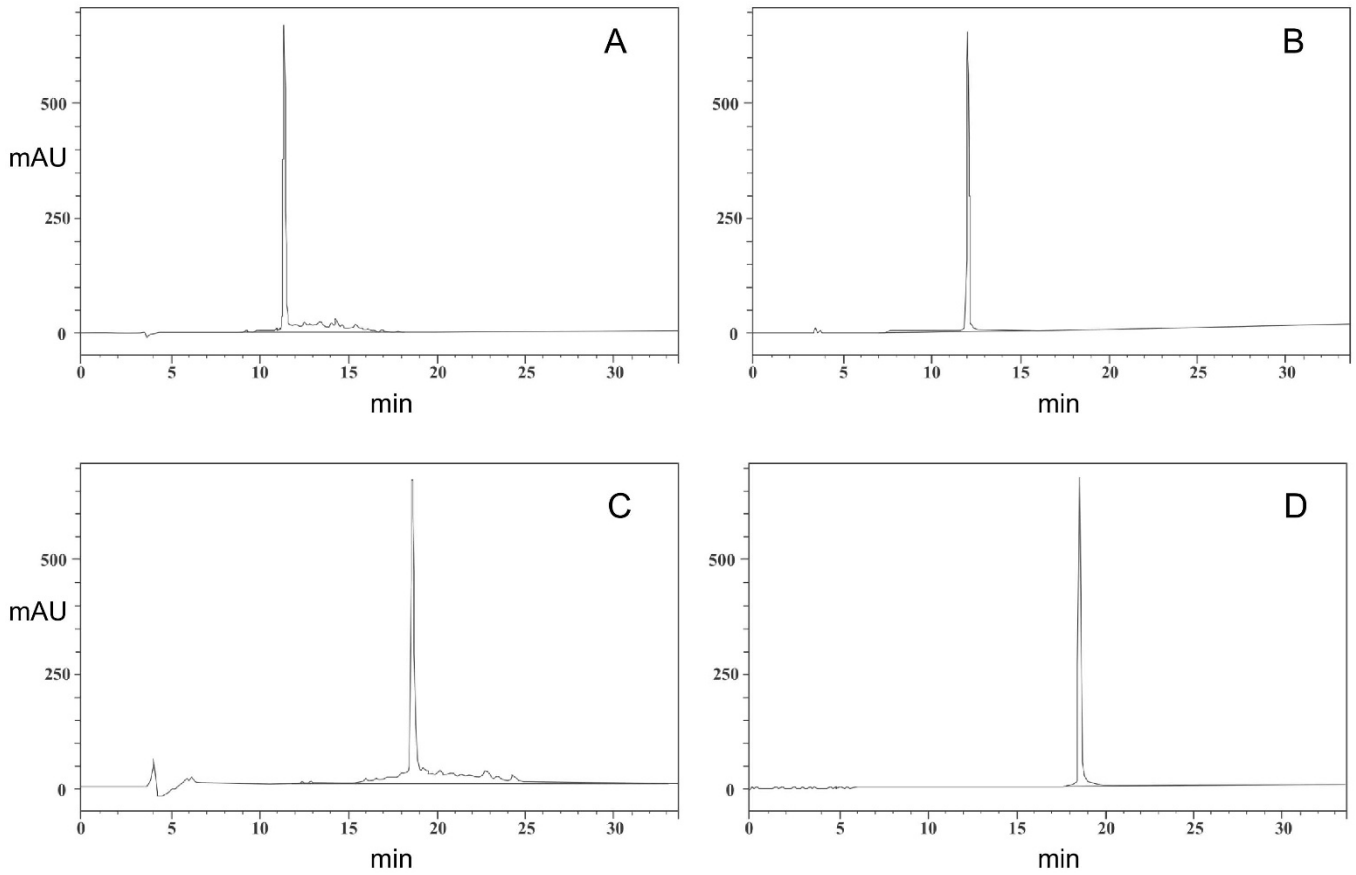

Figure 4 | Analysis of HsTX1 and HsTX1[R14A]. RP-HPLC profiles for the crude refolded HsTX1 (A) and HsTX1[R14A] (C), and purified refolded HsTX1 (B) and HsTX1[R14A] (D). The gradient was from 10–40% B in 30 min at a flow rate of 1 mL/min. Buffer A was 0.05% TFA in H_2O and Buffer B was 0.05% TFA in MeCN. The A_{220} was monitored for peak elution.

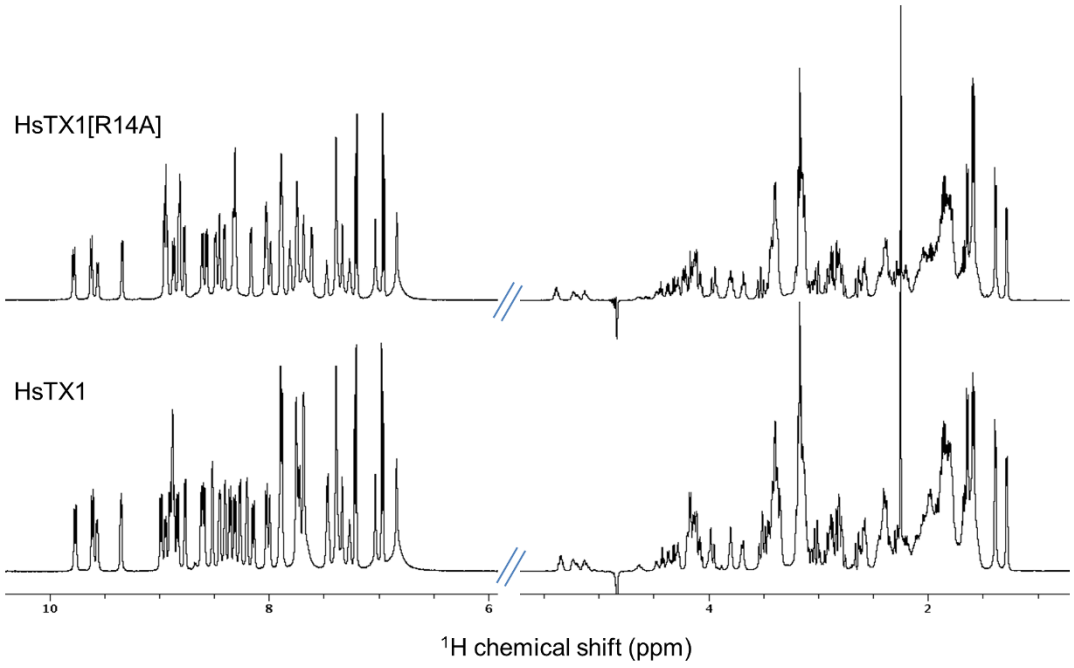

Figure 5 | Conformation of HsTX1[R14A]. Comparison of 1D ^{1}H NMR spectra of wild-type HsTX1 (bottom) and HsTX1[R14A], both in water at pH 4.0, and acquired on a Bruker Avance 600 MHz spectrometer at 35°C. The amide-aromatic regions of both spectra are expanded 2.5-fold vertically relative to the aliphatic regions.

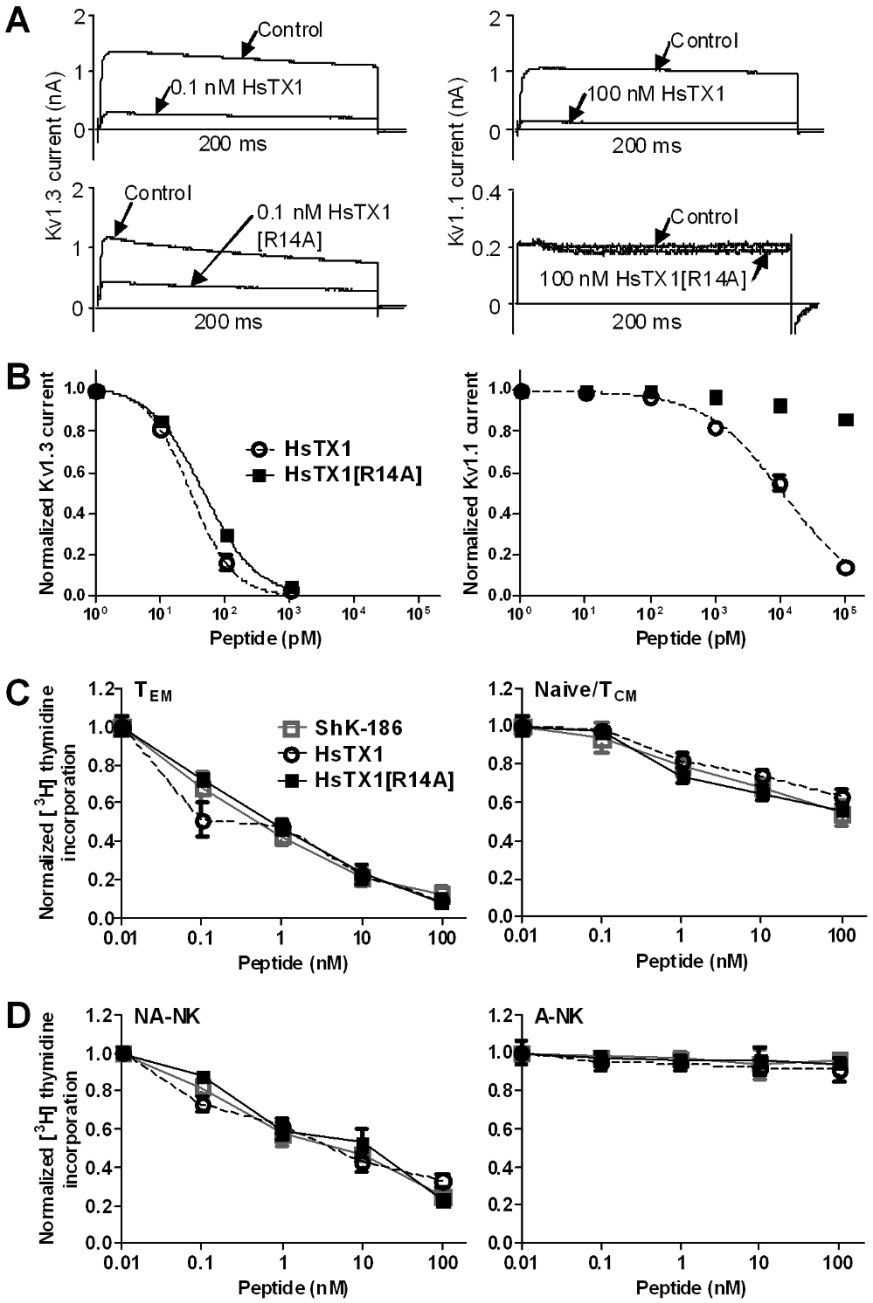

Figure 6 | Functional analyses of HsTX1[R14A]. (A) Whole-cell Kv1.3 (left) and Kv1.1 (right) currents measured by patch-clamp in stably transfected L929 fibroblasts before (control) and after perfusion of HsTx-1 (top panels) or of HsTX1[R14A] (bottom panels). (B) Dose-response inhibition of Kv1.3 (left) and Kv1.1 (right) currents by HsTX1 (○ and dashed line) and HsTX1[R14A] (■) fitted to a Hill equation (N = 3 cells per concentration). (C) Effects of ShK-186 (□ and grey line), HsTX1 (○ and dashed line), and HsTX1[R14A] (■) on the proliferation of rat Ova-GFP T_{EM} lymphocytes (left) and of rat splenic T lymphocytes [mainly naïve/T_{CM} cells] (right) measured *ex vivo* by the incorporation of [^{3}H] thymidine in the DNA of dividing cells (N = 3). (D) Effects of ShK-186 (□ and grey line), HsTX1 (○ and dashed line), and HsTX1[R14A] (■) on the proliferation of human NA-NK (left) and A-NK (right) lymphocytes (N = 3).

by α-chymotrypsin and trypsin (Fig. 7B,C) after 4 h at 37°C even though HsTX1[R14A] contains numerous basic and aliphatic residues that represent potential sites of cleavage.

We also investigated whether these peptides caused any haemolysis in human erythrocytes. As shown in Fig. 7D, none of the peptides displayed haemolytic activity when tested at doses of 100 nM.

Discussion

We have created several analogues of the scorpion toxin HsTX1 in which Arg14 is replaced with non-polar aliphatic or aromatic residues. HsTX1[R14A] retains high affinity for Kv1.3 (IC_{50} = 45 ± 3 pM) and exhibits more than 2,000-fold selectivity for Kv1.3 over Kv1.1. As selectivity for Kv1.3 over Kv1.1 is an important criterion for potential therapeutic applications in the treatment of autoimmune disease in humans[3,4], this peptide shows considerable promise as a new potential therapeutic lead.

With four disulfide bridges, HsTX1 has the potential to generate 105 distinct disulfide isomers during oxidative refolding in vitro. Our results for both the native peptide and HsTX1[R14A] show, however, that refolding is highly efficient and yields a single major isomer in good yield. In fact the presence of four disulfide bridges proves to be a significant benefit as the folded peptide is highly stable over a range of

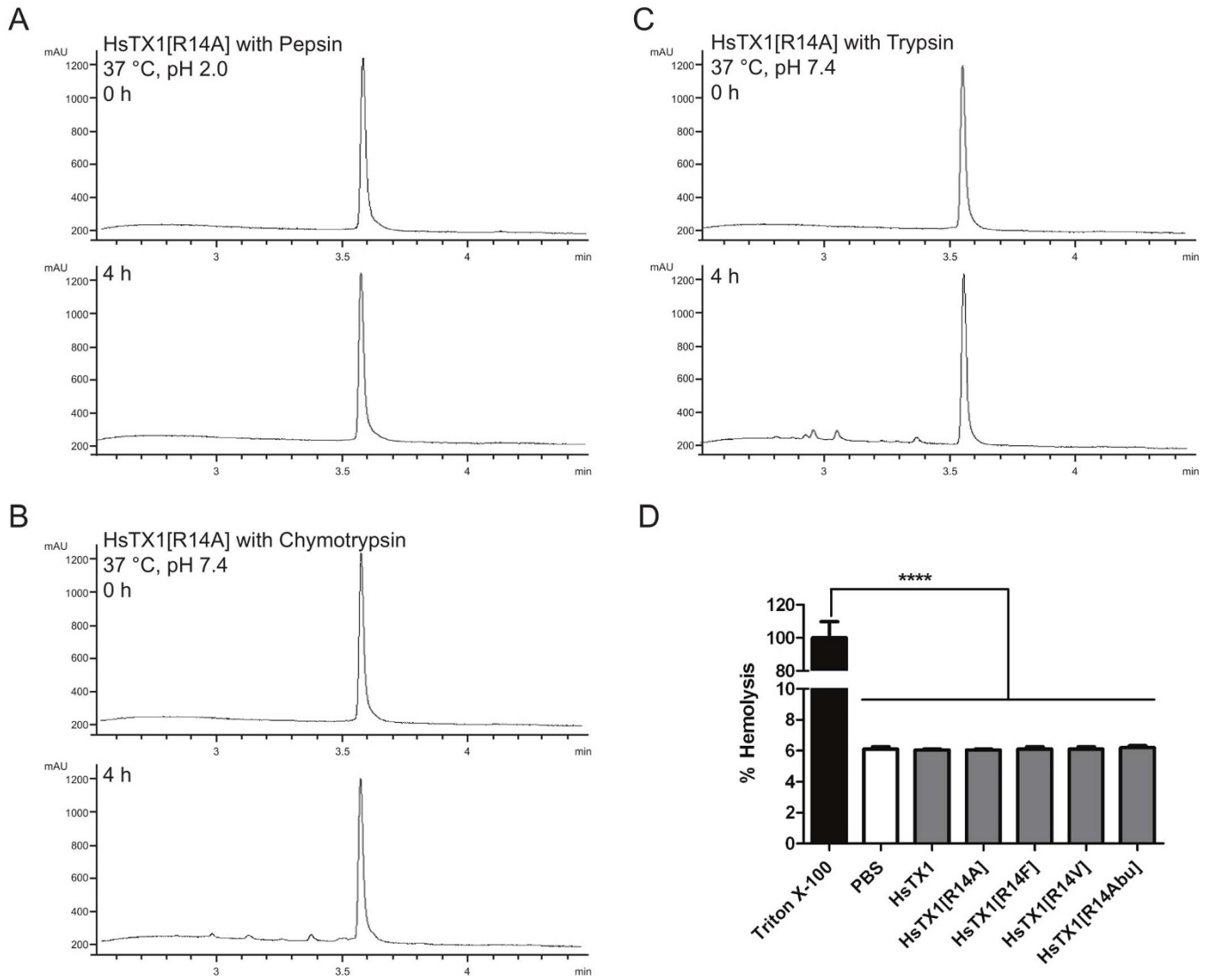

Figure 7 | Stability of HsTX1[R14A]. Reversed-phase HPLC analysis after treatment with pepsin (A), α-chymotrypsin (B) and trypsin (C). (D) Haemolysis assay; comparison of the haemolytic ability of HsTX1 and its analogues to haemolysis induced by Triton X-100 indicates that neither HsTX1 nor its analogues induces significant haemolysis. Data shown as average ± SEM (N=3).

pH and temperature in aqueous solution (our unpublished results). Consistent with this stability, HsTX1[R14A] is resistant to proteolysis by pepsin and showed only limited susceptibility to trypsin and chymotrypsin. There is an increasing acceptance of peptides as drug candidates[17] and an analogue of the sea anemone peptide ShK[3,4] has recently entered clinical trial for autoimmune diseases[11], so the therapeutic prospects for a potent, selective and stable peptide such as HsTX1[R14A] are quite promising. Analogues of other scorpion toxins also show promise in this respect, for example an engineered analogue of the three-disulfide-containing peptide BmKTX[18]. The finding that R14 analogues of HsTX1 preferentially inhibit the proliferation of $CCR7^-$ T_{EM} lymphocytes and NA-NK lymphocytes, leaving $CCR7^+$ naïve/T_{CM} and A-NK cells able to perform their normal functions, suggests that our HsTX1 analogues do not affect KCa3.1 channels and will not induce generalized immunosuppression.

The novel HsTX1 analogues described here display a remarkable selectivity for Kv1.3 over Kv1.1 channels. Homotetramers of the Kv1.3 channels have a discrete tissue distribution, with expression in lymphocytes and the olfactory bulb[19]. In other tissues expressing the Kv1.3 subunit, the resulting channel is a heterotetramer of different Kv1.x subunits. Selective blockers of Kv1.3 homotetramers are likely not to affect heterotetrameric channels and are expected to display no or few side effects, as was observed with the ShK analogue ShK-186[3,4,11]. In addition, as similar peptides do not cross the blood-brain barrier, HsTX1 and its analogues are unlikely to reach and affect Kv1.3 homotetramers in this tissue.

Our results also provide an excellent illustration of the predictive power of MD simulations and umbrella sampling PMF calculations, and how they can be exploited to design peptide analogues with enhanced selectivity properties[8,9,14] Because experimental structures for protein-ligand complexes are lacking in most cases, accurate construction of a complex structure using docking and MD simulations is of critical importance as it provides a basis for engineering modified peptides. In the next step, the free energy change associated with a given mutation can be accurately calculated using either the PMF method or free energy perturbation if the binding mode is preserved. In HsTX1, comparison of its binding modes with Kv1.1 and Kv1.3 almost uniquely identified R14A as a mutation that should improve the Kv1.3/Kv1.1 selectivity, and this was supported by the calculated binding free energies and confirmed by the measured binding constants.

Methods

Modelling and docking. Here we provide a brief description of the computational methods and refer to our previous work[13,14] for details. The structure of HsTX1[R14A] was generated from that of HsTX1 using the mutator plugin in the VMD software[20]. Because the affinity of HsTX1 for Kv1.2 is already below the measurement threshold, and R14A would reduce the toxin's affinity for Kv1.2 further, we consider here only the complexes with Kv1.1 and Kv1.3.

For the Kv1.1 and Kv1.3 structures, we used homology models based on the Kv1.2 structure, which were developed in[14]. The initial poses for the Kv1.x–HsTX1 complexes were found using the docking program HADDOCK[21], and then refined in MD simulations. The most stable complex in each case was further run for 20 ns to check equilibration and for data analysis. MD simulations were performed using the NAMD program[22] with the CHARMM36 force field[23]. The PMF of each toxin was determined from the umbrella sampling MD simulations using the weighted histogram analysis method[14,24].

The binding constant was determined from the integral of the PMF, $W(z)$, along the reaction coordinate using equation 1

$$K_{eq} = \pi R^2 \int_{z1}^{z2} e^{-W/kT} dz \quad (1)$$

Here z_1 was in the binding pocket and z_2 in the bulk where W vanishes. The factor πR^2 measures the cross sectional area of the binding pocket. The standard binding free energy of the toxin was obtained from equation 2

$$G_b = -kT \ln\left(K_{eq} C_0\right) \quad (2)$$

where C_0 is the standard concentration of 1 M.

Peptide synthesis. HsTX1 was synthesized on a Prelude peptide synthesizer using an Fmoc-tBu strategy. The peptide was synthesized starting with Rink amide resin (Peptides International, Louisville, KY). Prior to coupling the Arg at position 14, the resin was split into equal portions replaced into separate reaction vessels and coupled with either Arg, Ala, Phe, Abu, or Val. The remainder of the sequence was subsequently continued until the full length peptide was assembled. All couplings were mediated with diisopropyl carbodiimide and 6-chloro-hydroxybenzotriazole. Following solid-phase assembly of the linear peptide chain, the peptide was cleaved from the solid support and simultaneously deprotected using Reagent K for 2 h at room temperature. The crude peptide was precipitated into ice cold diethyl ether and washed thoroughly to remove cationic scavengers from the cleavage cocktail, dissolved in 50% aqueous acetic acid, then diluted in water and the pH adjusted to 8.0 with NH_4OH. Disulfide bond formation was facilitated with reduced and oxidized glutathione according to previously used protocols for ShK[10,15].

The progress of folding was followed by RP-HPLC using a Phenomenex Luna C18 column using a gradient of acetonitrile versus H_2O containing 0.05% TFA from 10–70% over 35 min. Folding of the three disulfide bonds was also confirmed by the loss of 6 mass units from the crude material as determined by ESI-MS.

NMR spectroscopy. Samples were prepared by dissolving lyophilised HsTX1 and HsTX1[R14A] in 90% H_2O/10%^2H_2O, pH 4.0, to concentrations of 500 and 400 μM, respectively. One-dimensional ^1H spectra and two dimensional homonuclear TOCSY spectra with a spin lock time of 70 ms were acquired at 35°C on a Bruker Avance 600 MHz spectrometer. A NOESY spectrum (mixing times 200 ms) was also acquired at 35°C. All spectra were processed in TOPSPIN (version 3.2, Bruker Biospin) and analysed using CcpNmr-Analysis (version 2.1.5). ^1H chemical shifts were referenced to the residual water signal. Chemical shift assignments for backbone and side chain protons of HsTX1[R14A] were made by conventional analysis of TOCSY and NOESY spectra. A complete assignment of the ^1H NMR resonances of HsTX1[R14A] was obtained.

CD spectroscopy. HsTX1 and HsTX1[R14A] were dissolved in 10 mM acetate buffer at pH 3.8 and CD spectra were recorded on a Chirascan v4.2.12 spectropolarimeter at concentrations of 94 and 89 μM, respectively, at 20°C. Spectra were collected at 1 nm intervals over the wavelength range 260–190 nm in a 1 mm path-length cuvette.

Cells and cell lines. Mouse L929 fibroblasts stably transfected with mKv1.1 or mKv1.3[25] were kind gifts from Dr. K. George Chandy (University of California, Irvine, USA).

$CD45RC^-CCR7^-$ ovalbumin-specific Ova-GFP T_{EM} lymphocytes were derived from Lewis rats by Dr. Flügel (University Medical Center Göttingen, Germany)[26]. They were maintained in culture through alternating rounds of expansion in cytokine-rich medium and antigen-induced activation; as antigen-presenting cells for the Ova-GFP T_{EM} lymphocytes, we used irradiated Lewis rat thymocytes[27]. Lewis rat splenocytes were isolated using Histopaque-1077 gradients from the thymus donors[28]. All procedures involving vertebrates were conducted under a protocol approved by the Institutional Animal Care and use Committee at Baylor College of Medicine. Female Lewis rats (7–9 weeks old) were purchased from Charles River Laboratories (Hollister, CA) and housed with food and water *ad libitum* in a facility approved by the Association for Assessment and Accreditation of laboratory Animal Care International (AAALAC). Rats were euthanized by deep anesthesia followed by cardiac puncture. Death was ensured by decapitation.

Buffy coats were purchased from the Gulf Coast Regional Blood Center (Houston, TX) and NK lymphocytes were further isolated by negative selection using the RosetteSep kit (Stemcell Technologies, Vancouver, Canada)[29]. Cells were incubated overnight in medium supplemented with 500 IU/ml IL-2 and 1 ng/ml IL-15 for separation of adherent and non-adherent NK cells[16]. The Institutional Review Board at Baylor College of Medicine determined that this work does not constitute human subject research as all buffy coats were de-identified and coded to preclude tracing a sample back to its donor.

Electrophysiological analysis. Patch-clamp experiments were conducted in the whole-cell configuration using either a manual setup or a Nanion Port-a-Patch setup, both connected to an EPC10-USB amplifier[9,25]. Chip or pipet resistances averaged 2 MΩ and the holding potential was set to −80 mV. Series resistance compensation of 80% was used when currents exceeded 2 nA. Kv currents were elicited by repeated 200 ms pulses from −80 to 40 mV, applied every 30 s, in normal Ringer solution with a calcium-free pipette buffer containing (in mM): 145 KF, 10 HEPES, 10 EGTA, 2 $MgCl_2$, pH7.2, 300 mOsm. IC_{50} values were determined by fitting the Hill equation to the reduction of area under the curve measured at 40 mV.

Lymphocyte proliferation assays. Effects of HsTX-1, HsTX-1[R14A], and ShK-186 on the proliferation of lymphocytes were measured by [^{3}H] thymidine incorporation assay in 96-well plates, as previously described[16,30]. Rat splenic mononuclear cells were plated at 10^5 cells/well; Ova-GFP T_{EM} cells at 50,000 cells/well in the presence of irradiated thymocytes (2×10^6/well); and adherent or non-adherent natural killer cells at 50,000 cells/well. The Kv1.3 blocking peptides were incubated with the cells for 30 min at 37°C before addition of the stimuli (1 μg/mL concanavalin A for splenic T cells, 10 μg/mL ovalbumin for Ova-GFP T_{EM} cells, and 40 ng/mL PMA + 500 nM ionomycin for NK cells). Cells were incubated for a total of 72 h at 37°C and [^{3}H] thymidine was added to the wells 16–18 h before harvesting of DNA on glass filters and counting of incorporated [^{3}H] thymidine using a β-scintillation counter (Beckman Coulter, Brea, CA).

Proteolysis assays. Proteolysis assays were performed at a 250 : 1 substrate (peptide)/enzyme ratio with pepsin, trypsin and α-chymotrypsin. For all assays, peptides were incubated with enzyme at 37°C for 4 h. As a positive control to ensure that active enzyme was present, bovine serum albumin was used as substrate in place of HsTX1[R14A]. All digestion assay data was analysed by reversed-phase HPLC (5–100% acetonitrile gradient, 10 min). Trypsin (EC 3.4.21.4, Sigma) and α-chymotrypsin (EC 3.4.21.1, Sigma), stocks were prepared in 50 mM Tris, 100 mM NaCl buffer (pH 7.4), and pepsin (EC 3.4.23.1, Sigma) stocks were prepared in 10 mM acetic acid/HCl buffer (pH 2). The trypsin and α-chymotrypsin reactions were halted with 2.5% acetic acid (25% v/v), and the pepsin reactions were halted with 2.5% of 200 mM glycine-NaOH buffer (pH 11).

Haemolysis assays. Erythrocytes were isolated from buffy coats obtained from the Gulf Coast Regional Blood Center (Houston, TX), as described previously[31]. Isolated haematocrit was diluted in PBS and incubated for 24 h at 37°C with 100 nM of the experimental peptides in 96-well plates. Absorbance of cell supernatants was then measured at 450 nm using a Powerwave XS microplate spectrophotometer (Biotek Instruments, Winooski, VT, USA).

1. Wulff, H. *et al.* The voltage-gated Kv1.3 K^+ channel in effector memory T cells as new target for MS. *J Clin Invest* **111**, 1703–1713 (2003).
2. Beeton, C. *et al.* Kv1.3 channels are a therapeutic target for T cell-mediated autoimmune diseases. *Proc Natl Acad Sci U S A* **103**, 17414–17419 (2006).
3. Beeton, C., Pennington, M. W. & Norton, R. S. Analogs of the sea anemone potassium channel blocker ShK for the treatment of autoimmune diseases. *Inflamm Allergy Drug Targets* **10**, 313–321 (2011).
4. Chi, V. *et al.* Development of a sea anemone toxin as an immunomodulator for therapy of autoimmune diseases. *Toxicon* **59**, 529–546 (2012).
5. Lebrun, B. *et al.* A four-disulphide-bridged toxin, with high affinity towards voltage-gated K^+ channels, isolated from *Heterometrus spinnifer* (Scorpionidae) venom. *Biochem J* **328 (Pt1)**, 321–327 (1997).
6. Savarin, P. *et al.* Structural and functional consequences of the presence of a fourth disulfide bridge in the scorpion short toxins: solution structure of the potassium channel inhibitor HsTX1. *Protein Sci* **8**, 2672–2685 (1999).
7. Regaya, I. *et al.* Evidence for domain-specific recognition of SK and Kv channels by MTX and HsTx1 scorpion toxins. *J Biol Chem* **279**, 55690–55696 (2004).
8. Pennington, M. W. *et al.* A C-terminally amidated analogue of ShK is a potent and selective blocker of the voltage-gated potassium channel Kv1.3. *FEBS Lett* **586**, 3996–4001 (2012).
9. Rashid, M. H. *et al.* A potent and selective peptide blocker of the Kv1.3 channel: prediction from free-energy simulations and experimental confirmation. *PloS one* **8**, e78712 (2013).
10. Pennington, M. W. *et al.* Engineering a stable and selective peptide blocker of the Kv1.3 channel in T lymphocytes. *Mol Pharmacol* **75**, 762–773 (2009).
11. Norton, R. S., Pennington, M. W. & Beeton, C. [Transforming a toxin into a therapeutic: the sea anemone potassium channel blocker ShK toxin for treatment of autoimmune diseases] *Venoms to drugs: Venom as a source for the development of human therapeutics* [King, G. F. (ed.)] [in press] (Royal Society of Chemistry, London, 2014).

12. Rashid, M. H. & Kuyucak, S. Free energy simulations of binding of HsTx1 toxin to Kv1 potassium channels: the basis of Kv1.3/Kv1.1 selectivity. *J Phys Chem B* **118**, 707–716 (2014).
13. Chen, P. C. & Kuyucak, S. Accurate determination of the binding free energy for KcsA-charybdotoxin complex from the potential of mean force calculations with restraints. *Biophys J* **100**, 2466–2474 (2011).
14. Rashid, M. H. & Kuyucak, S. Affinity and selectivity of ShK toxin for the Kv1 potassium channels from free energy simulations. *J Phys Chem B* **116**, 4812–4822 (2012).
15. Pennington, M. W. *et al.* An essential binding surface for ShK toxin interaction with rat brain potassium channels. *Biochemistry* **35**, 16407–16411 (1996).
16. Koshy, S. *et al.* Blocking KCa3.1 channels increases tumor cell killing by a subpopulation of human natural killer lymphocytes. *PloS one* **8**, e76740 (2013).
17. Craik, D. J., Fairlie, D. P., Liras, S. & Price, D. The future of peptide-based drugs. *Chem Biol Drug Des* **81**, 136–147 (2013).
18. Han, S. *et al.* Structural basis of a potent peptide inhibitor designed for Kv1.3 channel, a therapeutic target of autoimmune disease. *J Biol Chem* **283**, 19058–19065 (2008).
19. Gutman, G. A. *et al.* International Union of Pharmacology. XLI. Compendium of voltage-gated ion channels: potassium channels. *Pharmacol Rev* **55**, 583–586 (2003).
20. Humphrey, W., Dalke, A. & Schulten, K. VMD: visual molecular dynamics. *J Mol Graph* **14**, 33–38 (1996).
21. Dominguez, C., Boelens, R. & Bonvin, A. M. HADDOCK: a protein-protein docking approach based on biochemical or biophysical information. *J Am Chem Soc* **125**, 1731–1737 (2003).
22. Phillips, J. C. *et al.* Scalable molecular dynamics with NAMD. *J Comput Chem* **26**, 1781–1802 (2005).
23. Klauda, J. B. *et al.* Update of the CHARMM all-atom additive force field for lipids: validation on six lipid types. *J Phys Chem B* **114**, 7830–7843 (2010).
24. Kumar, S., Bouzida, D., Swensen, R. H., Kollman, P. A. & Rosenberg, J. M. The weighted histogram analysis method for free-energy calculations on biomolecules. *J Comput Chem* **13**, 1011–1021 (1992).
25. Grissmer, S. *et al.* Pharmacological characterization of five cloned voltage-gated K^+ channels, types Kv1.1, 1.2, 1.3, 1.5, and 3.1, stably expressed in mammalian cell lines. *Mol Pharmacol* **45**, 1227–1234 (1994).
26. Flugel, A., Willem, M., Berkowicz, T. & Wekerle, H. Gene transfer into $CD4^+$ T lymphocytes: green fluorescent protein-engineered, encephalitogenic T cells illuminate brain autoimmune responses. *Nat Med* **5**, 843–847 (1999).
27. Matheu, M. P. *et al.* Imaging of effector memory T cells during a delayed-type hypersensitivity reaction and suppression by Kv1.3 channel block. *Immunity* **29**, 602–614 (2008).
28. Beeton, C. & Chandy, K. G. Preparing T cell growth factor from rat splenocytes. *J Vis Exp* **10**, 402 (2007).
29. Beeton, C. & Chandy, K. G. Enrichment of NK cells from human blood with the RosetteSep kit from StemCell technologies. *J Vis Exp* **8**, 326 (2007).
30. Chang, S. C. *et al.* Expression and isotopic labelling of the potassium channel blocker ShK toxin as a thioredoxin fusion protein in bacteria. *Toxicon* **60**, 840–850 (2012).
31. Evans, B. C. *et al.* Ex vivo red blood cell hemolysis assay for the evaluation of pH-responsive endosomolytic agents for cytosolic delivery of biomacromolecular drugs. *J Vis Exp* **73**, e50166 (2013).

Acknowledgments

This work was supported in part by National Institutes of Health grants NS073712 (to CB, MWP and RSN) and GM088129 (to MRT). RSN acknowledges the award of a fellowship by the National Health and Medical Research Council of Australia. We thank John Gehman for assistance with CD spectroscopy. Calculations were performed using the HPC facilities at the National Computational Infrastructure (Canberra).

Author contributions

M.H.R. performed the computations, M.H.R. and S.K. analysed the data, R.H., M.R.T. and C.B. performed the electrophysiology, proliferation and heamolysis assays, S.C. recorded and analysed NMR and CD spectra, R.E., V.D. and S.C. synthesized and purified the peptides, and K.K.K. and S.C. performed the proteolysis studies. S.K. and R.S.N. conceived the study and M.W.P., C.B., S.K. and R.S.N. wrote the paper with input from all authors.

Additional information

Supplementary information accompanies this paper at http://www.nature.com/scientificreports

Competing financial interests: The authors declare no competing financial interests.

How to cite this article: Rashid, M.H. *et al.* A potent and Kv1.3-selective analogue of the scorpion toxin HsTX1 as a potential therapeutic for autoimmune diseases. *Sci. Rep.* **4**, 4509; DOI:10.1038/srep04509 (2014).